Article:
Antony, SJ, Al-Sharabi, M, Rahmanian, N et al. (2015) Shear stress distribution within narrowly constrained structured grains and granulated powder beds. Advanced Powder Technology, 26 (6). pp. 1702-1711. ISSN: 0921-8831

https://doi.org/10.1016/j.apt.2015.10.011

Shear stress distribution within narrowly constrained structured grains and granulated powder beds

S.J. Antony[1]*, M. Al-Sharabi[1], N. Rahmanian[2] and T. Barakat[3]

[1] *School of Chemical and Process Engineering, University of Leeds, LS2 9JT, UK*
[2]*School of Engineering, Faculty of Engineering and Informatics, University of Bradford, Bradford, BD7 1DP, UK*
[3] *Department of Physics and Astronomy*, *College of Science, King Saud University, PO Box 2455, Riyadh, Saudi Arabia*

Abstract

An experimental study is presented here to understand the stress transmission characteristics under different geometrical arrangements of particulates inside a narrow chamber subjected to axial compression loading. The multi-grain systems considered here are face-centred, simple cubic and poly-dispersed structures, as well as inclusions embedded inside seeded, unseeded and cohesive powder bed of Durcal (calcium carbonate). The distribution of the maximum shear stress, direction of the major principal stress and shear stress concentration factor were obtained using photo stress analysis tomography (PSAT). The results show that the maximum shear stress distribution in the simple cubic structure is chain-like and self-repetitive, i.e, a single grain behaviour is representative of the whole system. This is not the case in the case of other granular packing. In the case of the inclusion surrounded by powder media, the maximum shear stress distribution in the inclusion occurs through ring-like structures, which are different from those observed in the structured granular packing. This tendency increases for an increase in the cohesivity of the surrounding particulates. In the granular systems, the direction of the major principal stress is mostly orthogonal to the direction of loading except in some particles in the random granular packing. In the case of inclusion surrounded by Durcal particulates, the directional of the major principal stress acts along the direction of the axial loading except in the ring region where this tends to be oblique to the direction of axial loading. Estimates of the shear stress concentration factor (k) show that, k tends to be independent of the structural arrangement of granular packing at higher load levels. In the case of inclusion surrounded

by powder bed, k for the seeded granulated particulate bed is mostly independent of the external load levels. In the case of unseeded particulate (granulated) bed, a fluctuation in k is observed with the loading level. This suggests that the seeded granules could distribute stresses in a stable manner without much change in the nature of shear stress-transmitting fabric of the particulate contacts under external loading. An increase in the cohesion of particulate bed results in more plastic deformation as shown by the differential shear stress concentration factor. The results reported in this study show the usefulness of optical stress analysis to shed some scientific lights on unravelling some of the complexities of particulate systems under different structural arrangements of grains and surrounding conditions of the inclusions in particulate media.

Keywords: Particulate media, granular materials, powders, micromechanics, photo stress analysis tomography, structured materials

* Corresponding author: S.J.Antony@leeds.ac.uk Ph.: 00441133432409

1 Introduction

Particulate materials such as grains and powders are encountered in several industrial applications, for example, chemical, petroleum, pharmaceutical, food, geotechnical, minerals and materials processing sectors [1]. Granular materials consist of discrete solid particles that are arranged in a random or a particular structural form [2]. Such materials have a complex heterogeneous mechanical behaviour under different loading conditions [3]. Understanding the micromechanical behaviour of granular assemblies of different packing structure is important in engineering processes from molecular to bulk scales such as metals [4], crushing [5], permeability [6], erosion [7], composites [8] and granular physics [9-11]. The internal structural (fabric) arrangement of grains has a significant impact on their bulk behaviour under various mechanical loading environments [12-19].

Micromechanical analysis of fine particulate systems, especially stress measurements in particulates, is performed by theoretical and computational studies [20]. The micromechanical behaviours of granular materials have been studied using discrete element method (DEM) [5, 17, 21-23]. However, DEM does not account for the stress transmission within the individual grains at a single particle scale [24]. Furthermore, in general, DEM simulations do not account for the interaction effects of a particular contact on the stress transmitted by its neighbouring contacts. Some studies have used coupled DEM-FEM (Finite Element Method) analysis to get information on the stress distribution within individual particles in particulate assemblies [25] but these studies are computationally expensive. Some experimental studies have used indentation methods on the outer surface of powder beds and interpreted the indentation depths to their material properties [26]. Experimental measurement of stresses inside particulate beds is difficult to conduct at the present time. However, recent studies show the usefulness of photo stress analysis tomography (PSAT) for obtaining the stress distribution within inclusions in particulate systems [1]. These studies have used optical stress analysis for understanding the mechanical response of fine particulates interacting with optically stress-sensitive inclusions and their surroundings (Antony et al, 2015). They provide new understandings on the ability of particulates to distribute shear under mechanical loading. However, information on the shear stress distribution characteristics of some structures such as face-centred (FC), simple cubic (SC) and poly-dispersed systems within constrained walls (narrow channels in which distance between the walls is comparable to the size of the particle) are not yet well studied, but addressed in this paper. Furthermore, the shear stress distribution characteristics within inclusions surrounded by constrained granules made of fine powders through different manufacturing routes are not yet fully understood. For example, a new method of granulation was recently introduced as 'seeded granulation' [27]. In this process, large particles present in the feed act as seeds in the granulation. Seeded granules refer to the granules having the largest particle at the centre of the granule and unseeded granules do not have this feature. It has been shown that seeded granulation produces granules with narrower distributions of granule size, uniform strength, structure and density. Observations by X-ray micro-tomography and

scanning electron microscopy (SEM) of sectioned granules show that under optimum conditions, each granule contains a seed at its centre [27-29]. Figure 1a and 1b show X-ray micro-tomography images of the central cross section of two different granules re-produced here, which illustrate seeded and unseeded granules respectively. The white coloured material appeared at the centre of granule in Fig.1a is a single crystal of Durcal (calcium carbonate) and this type of granule possesses higher strength and lower porosity than the granule in Fig.1b (unseeded). The mechanism of formation of seeded granules is not yet fully understood due to the complex nature of shear response of particulates to external loading environments. In fact, we are still away from sensing stress distribution inside a powder bed at any point of interest. In granulation processes, the mechanics of particle interactions and the prevailing level of compressive and shear stresses at single particle level and bulk scales are affected by the operating conditions, scale of operation and product formulation, which in turn affect the granule properties, but they are not largely understood. Figure 2 shows the SEM image of Durcal 65 powder. It is not known how mechanical properties of such powder systems get influenced by constrained external compression loading, and what parameter of any experimentally sensed shear stress state could reflect the bulk response of the powder bed. In the present paper, unlike intending the particulate beds at their external boundaries to assess their mechanical response [26], a birefringent inclusion is placed inside the bed. By sensing the stress distribution characteristics of the inclusion under mechanical loading, interesting observations can be made on the ability of the surrounding particulates to transmit shear through the inclusion (which acts as a stress sensor) using PSAT. These challenges are addressed below.

2 Background of Photo Stress Analysis

Photo elastic studies have been carried out in the past to examine the stress distribution characteristics of granular materials under external loading [1, 9, 30-32]. Stress distribution characteristics such as the variations of maximum shear stress, principal stress directions and shear stress concentration factor

can be obtained using PSAT technique. A schematic diagram of the configuration of a circular polariscope used for PSAT experiments is shown in Fig.3 [24]. The working principle of PSAT is based on an optical phenomenon called birefringence [30]. The application of stress on a birefringent material alters its refraction index. Hence, the electromagnetic wave components of the polarised light experience a double refraction upon its passage through the birefringent material as a result of the different refraction indices. This results in a phase retardation of light, which can be characterised by fringe patterns of different orders and then further analysed to obtain the distribution of maximum shear stress in birefringent materials [1]. The relationship between the induced light retardation (Δ), change in the major (σ_{11}) and minor (σ_{33}) principal stresses and fringe order (N) can be explained by the stress-optic laws expressed as follows [30];

$$\Delta = \frac{2\pi t}{\lambda} C(\sigma_{11} - \sigma_{33}) \qquad (1)$$

$$N = \frac{\Delta}{2\pi} \qquad (2)$$

where;

$t =$ thickness of specimen (m)

$\lambda =$ wavelength (nm)

σ_{11}-σ_{33} = difference between the principal stresses (Pa)

$C =$ stress optic coefficient $(\frac{\frac{nm}{m}}{Pa})$

The above equations can be represented in a simple form as [30];

$$\sigma_{11}-\sigma_{33} = Nf_\sigma/t \qquad (3)$$

in which, f_σ is the material stress fringe constant (N/m-fringe). By measuring the fringe order at a point of interest on the model, the difference between the principal stresses (and hence the maximum

shear stress) can be calculated using the above said equations [30]. The direction of the major and minor principal stresses can be obtained using a plane polariscope setup and the details can be found elsewhere [30].

3 Experiments

The material properties of the birefringent disk (circular) used in this study is summarised in Table 1. Two types of particulate systems are considered in this study (Fig.4). Type 1: granular systems of face centred (FC) and simple cubic (SC) structures with 20mm diameter grains, random granular structure (poly-dispersed) with diameter 20mm (3 grains), 25mm (6 grains) and 30mm (3 grains) and Type-2: particulate systems of inclusions embedded in seeded granules (Fig.1a), unseeded granules (Fig.1b) and for comparison purposes Durcal 65 powder (Fig.2); i.e., calcium carbonate powder manufactured by Omya UK Ltd. Solid density of the powder is 2750 kg/m^3 and characteristics of particle size distribution of the powder obtained by Mastersizer 2000 (Malvern, UK) is d_{10}=7μm, d_{50}=63μm and d_{90}=225μm. As it shows, the powder particles have irregular shape. The granulated powder material used polyethylene glycol (PEG) as a binder. The manufacturing of seeded and unseeded granules depends on the impeller speed of the granulator and the primary particle size. The granulated and powder bed samples used in this study are the same as reported by Rahmanian et al. [27]. The details of manufacturing the seeded and unseeded granules and their physical properties are explained in detail in the previous work [27, 28] and briefly discussed below.

The method for the production of seeded granules in a batch process has been demonstrated in four different scales of Cyclomix high shear mixer granulators (Manufactured by Hosokawa Micron, B.V., the Netherlands) with capacities from laboratory scale, 1 and 5 L, to pilot plant scale of 50 L and finally to industrial scale of 250 L [33]. Different commercial grades of calcium carbonate, coarse particles (Durcal 65) and finer particles (Durcal 40 having d_{10}=8μm, d_{50}=43μm and d_{90}=92μm and

Durcal 15 with d_{10}=2µm, d_{50}=23µm and d_{90}=64µm) were selected as model materials. Aqueous PEG was used as the binder. Figure 1a shows an X-ray micro-tomography image of the central cross section of a granule produced by the above method. Figure 1c shows the internal structure of about 100 granules probed using SEM. The SEM image shows the seeded granules embedded in a resin on a plane and cut and polished to show their internal structure. Every granule has consistently a seed, which is a large particle from the top end of the size distribution of the feed powder [27].

We assessed the angle of repose [34] and crushing force of them for an indication of their cohesiveness and strength respectively and the results are presented in Table 2. Crushing strength was measured using Mach-1^{TM} Micromechanical System (Canada). The test was carried out with the equipment set at a maximum load of 10 kg and a loading velocity of 0.05mm/s. At least 30 granules per sample were randomly selected and tested, and then the average and standard deviation of crushing strength was determined to ensure the reliability of the results. This procedure test is similar to the reported work by Rahmanian et al. [28], where they used a different device; i.e. Instron to characterise strength of granules.

The loading rig used for investigating the stress distribution characteristics under compression is illustrated in Fig.5. In the case of the inclusion surrounded by the powder bed, the thickness of the powder bed and the inclusion are the same (6mm). The circular inclusion (20mm diameter) is positioned at the middle of the bed. The particles were filled in several layers gradually to minimise any segregation of the granules. The same protocol is used to make the filling identically as much as possible in all the three cases of the powder bed. The samples were placed in the loading rig and subjected to axial compression under different load levels. The images of the optical fringes for the different particulate systems at different load levels were captured digitally [35] and analysed to obtain the maximum shear stress distribution, direction of the major principal stress and shear stress concentration factor [36].

4 Analysis

The fringe order measurements were taken at several points of the birefringent grains and the inclusions. Using this, contours of the distribution of maximum shear stress and direction of the major principal stress were generated for the assemblies under the different external loading conditions. Furthermore, the shear stress concentration factor (k) was evaluated by scanning the shear stress data along the selected section in the birefringent particle as follows:

$$\text{Shear stress concentration factor } k = \frac{\tau_{max}}{\tau_{avg}} \quad (4)$$

$$\text{Coefficient of variation CV} = \frac{Standard\ deviation\ of\ \tau_{max}}{\tau_{avg}} \quad (5)$$

where, τ_{max} is the highest value of maximum shear stress acting along the chosen section.

τ_{avg} is the average value of the maximum shear stress acting along the chosen section.

Here, the values of τ_{max} and τ_{avg} were obtained by scanning the birefringent particle in the vertical direction along the axis of the compressional loading as illustrated in Fig.6. CV is the relative index of the uniformity of shear stress distribution. The lower standard gives rise to a more homogenous stress distribution in the assembly.

5 Results and Discussion

Figure 7 shows the distribution of maximum shear stress within the particles in the FC, SC and random packing structures. It is evident that the magnitude of the maximum shear stress in all these three structural arrangements is proportional to the load level: increase in the external load level increases the level of shear stress in the systems. However, as shown in Fig.7, a few particles in the random packing (e.g. the middle particle in the top row) continue to be relatively weak in shear for an increase in the load level. This is consistent with the previous literatures [17, 37], which show that stress distribution in random granular structures occurs in a non-

homogeneous manner. Some particles transmit relatively strong forces while others share weak forces or no forces at all. What is intersting here is, such behaviour is also observed in the case of narrowly constrained random granular packing. Furthermore, when we compare the nature of the stress distribution between the FC and SC packing strctures, it is evident that the maximum shear stress distribution is transmitted through well connected chain-like structures. Futhermore, mostly identical (repetitive) stress distribution patterns are seen in all the particles of the SC packing. They also display symmetric stress distribution profiles with respect to the vertical axis passing through the centre the particles. In this case, unlike in the case of other structures, the characteristics of stress distribution in a single particle is representative of the whole system. In the case of inclusions inside the powder surroundigns (Fig.8), the nature of shear stress distribution is remarkably different from that of granular packing. The stress distribution patterns are not necessarily proportional to the external load level espcially in the cases of unseeded granules surrounding (lowest angle of repose). In the case of cohesive Durcal powder surrounding (highest angle of repose), ring-like maximum stress distribution patterns are evident in the inclsuions. This suggests that the increase in the cohesivity (angle of repose) of the particles tends to generate radially symmetrical stress distribution, although the particulate bed is subjected to axial compression loading. To emphasise this further, we present two typical images of shear stress distribution in Fig.9. One of the images corresponds to the inclsuion surrounded by the cohesive powder bed (P=41.9N). In the other case, the inclusion alone (without the surrounding powder bed) is subjected to axial compression loading (P=5.9N). The maximum shear stress distribution exhibits axial symmerty in the former case while in the latter case, the radial symmetry is evident in the inclusion. We wish to point out that a relatively higher level of loading was required to obeserve the fringe patterns in the inclsuions surrounded by the cohesive bed, as the cohesive particles sustain a relatively higher level of mechanical strength as anticipated. Hence, the stress exhibited in the inclusion also serves as an indicator of the strength of surrounding particulates.

Figures 10 and 11 illustrate the distribution of the direction of the major principal stress in the granular and powder bed systems under axial compression loading. For conveneince, this is presented in two forms, viz., contours, as well as in dotted lines for showing the direction of the major principal stress. What is evident is, by and large the granular systems distribute the major principal stress orthogonally to the direction of axial loading, barring some particles in the random packing. This is more evident in the case of SC granular packing, where all the particles distribute major principal stress othogonally to the direction of axial loading (similar to the well known behaviour of a single grain subjected to axial compression [38], also illustrated in the enlarged images of Fig.12 for comparison. On the other hand, the powder surrounding distribute the major principal stress along the direction of the axial loading except in the regions of the 'radial stress rings' (where the maximum shear stress is relatively high). In the rings, the major principal stress tends to be non-aligned with the direction of axial loading. This tendency increases for an increase in the cohesivity of the powders as evident from the far right column of the images presented in Fig.11. The variation of shear stress concerntration factor (k) is presented in Figures 13 and 14. We observe that, in the case of FC granular packing, k is relatively less dependant on the load level. For higher load levels, k tends to be independent of the granular packing structure. In the case of the inclsuion surrounded by seeded partiuclate bed, k is almost independent of the load level. Previous computational studies have shown that the microscopic origin of the shear strength in partiuclate systems could be attributed to the fabric anisotropy of particle conatcts under mechanical loading [17]. Hence, we could deduce that, as the variation in k is independent of the load levels in seeded particulates, their fabric structures (through which normally strong force transmisison occurs [17] could be more stable unlike in the case of unseeded system where some fluctuations in k are observed with the load level. However, further experimental studies are required in the future to quantify the fabric variations of inclsuions in partiuclate systems under mechanical loading. To understand the plastic deformation effect of the powder bed qaulitatively, we evaluated the differential k (Δk), which is the difference between the value of k evaluated

between the loading and unloading cycles with respect to the reference load level of 5.9N (the intial axial load level applied on the beds was 5.9N, then the loading progressed up to 82.1N in increments. Then, the unloading was done in steps until reaching the reference load level. The value of k was evaluated at the reference load level during the loading and unloading cycles, and Δk is the difference between them).

Figure 14 shows the coeffcient of variation (CV) of k for three different assemblies of powder bed versus load. The results are interesting. The fluctuation of CV for the unseeded bed can be an indication of high porsoity of these type of granules, see Fig.1a, and the fluctuations can be due to rearrangment of primary particles in the bed. This could also be an index of breakge of these granules due to high compression load as these are the weakest granules as comapred to the seeded structure granules. For the case of $CaCO_3$ powder bed, the trend of CV flattens at about 30N, which confirms the rigid structure of this assembly as this powder contains very fine particles. For seeded granules, the trend remains constant and the lowest CV for this type of granules is an indication of the relatively more uniform stress distribution for this bed. These results are corroborated with the results of strength measurment of these granules as they possess the highest strength as comapred to unseeded structure. The previous results [27] also show the most uniform strength and mechanical properties for this type of seeded structure as comapred to the unseeded structure.

From Fig.16, we observe that the absolute value of Δk, which is the difference between k values of the loading and unloading stages at the reference load level (5.9N), increases for an increase in the cohesivity of the particles. However, in the case of the particulate bed with the highest cohesion (Durcal powder bed), the value of k at the reference load level of the unloading cycle was higher than that of the loading cycle, and hence Δk was negative. This could happen in highly cohesive fine powder system where the plastic deformation gained during the loading cycle is

locked relatively more permanently. The seeded and unseeded granulated beds have bounced back relatively more than the Durcal powder bed with regard to k. The current approach is capable of enlightening such internal characteristics of particulates under mechanical loading more effectively. Further studies could assess such permanent lock-in structural effects of powders for other types of cohesive powders under different loading conditions.

6. Conclusions

In spite of the significant level of advancements reported by the worldwide research community, the micromechanical behaviours of particulate systems are still not well understood. One of the problems that contribute to this is the lack of experimental understandings on the stress transmission characteristics inside particulate systems. The results presented above help to understand the role of packing arrangement of particles on the shear stress distribution characteristics under external axial compression loading using photo stress analysis methodology. The study shows that the shear stress distribution profiles in the SC granular packing are chain-like and self-repetitive under axial compression: what happens in a single grain is a representation of the whole system. Also in this system, the profile of the direction of the major principal stress pertains to that of a single grain under axial compression. In the FC and random structured granular packing, the distribution of shear within the grains occurs non-uniformly. In the case of the inclusions surrounded by the Durcal particulate packing, ring-like structures of maximum shear stress distribution are observed. Such radial structures are more evident in the case of the highly cohesive powder surrounding. In this case, the direction of the major principal stress acts along the direction of the external loading in the inclusion except within the radial rings. The evaluation of shear stress concentration factor k of the particulate systems suggests that, (i) in the granular packing, k is almost independent of the granular packing structure at a relatively high load level. Based on the observations of k for the inclusions surrounded by Durcal particulate beds, we suggest that seeded particulates could sustain a more stable load-transmitting

fabric structure, and independent of the external loading levels. This is consistent with the experimental data reported earlier [27] that seeded granules are stronger than unseeded granules. Cohesive Durcal powder bed displays the highest level of structural plastic deformation as characterised by the differential shear stress concentration factor. Considering the complexities of sensing stresses for particulate media, the PSAT method applied here is promising. It provided valuable information, at least qualitatively, on the internal micromechanical features of different types of constrained packing under axial compression. However, further technological developments are required to experimentally quantify the nature of the fabric structures of load-transmitting contacts in fine particulate systems. Further studies are required to account for variables other than the ones considered in this study, such as different preparation methods of grains [39], wall roughness, shape effects of the grains and inclusions, size distribution of granulated particles or primary particles, their volumetric fraction, packing density and cohesivity of different types of fine particles on their micro and nano mechanical characteristics. It would be also interesting to explore the link between the coordination number of the granular packing to a suitably characterised distribution of force (/stress) components at inter-grain contacts [40], for which further information is required to partition the individual components of contact forces in the granular systems.

Acknowledgement

This Project was funded by the National Plan for Science, Technology and Innovation (MAARIFAH), King Abdulaziz City for Science and Technology, Kingdom of Saudi Arabia, Award Number (11-NAN-1877-02). The authors also thank Dr. G. Okeke for his support in conducting the experiments and Dr. Peter van der Wel from Hosokawa Micron B.V. (The Netherlands) for providing access to the Cyclomix granulator for preparing the granules.

References

[1] S.J. Antony, O. Imafidon, T. Barakat, Micromechanical analysis of inclusions in particulate media using digital photo stress analysis tomography, Opt. Eng., 54 (2015) 081202.

[2] M. Oda, K. Iwashita, Mechanics of Granular Materials, A.A.Balkema, Rotterdam, 1999.

[3] H. Arslan, G. Baykal, S. Sture, Analysis of the influence of crushing on the behaviour of granular materials under shear, Gran. Matt., 11 (2009), 87-97.

[4] R. Abbaschian, L. Abbaschian, R. Reed-Hill, Physical Metallurgy Principles, Wadsworth Publishing, California, 2009.

[5] A. Refahi, J.A. Mohandesi, B. Rezai, Comparison between bond crushing energy and fracture energy of rocks in a jaw crusher using numerical simulation, Jl.Sou.Afr.Inst.Min.Met., 109 (2009) 709-717.

[6] D.C. Beard, P.K. Weyl, Influence of texture on porosity and permeability of unconsolidated sand. Am.Ass.Pet. Geo. Bull., 57(1973), 349-369.

[7] F. Petit, Evaluation of grain shear stresses required to initiate movement of particles in natural rivers, Ear.Sur.Proc.Land., 15 (1990), 135-148.

[8] J. Liu, P. Ownby, Enhanced mechanical properties of alumina by dispersed titanium diboride particulate inclusions, Jl. Am. Cer. Soc., 74(1991) 241-243.

[9] I. Zuriguel, T. Mullin, J.M. Rotter, Effect of particle shape on the stress dip under a sandpile, Phy.Rev.Let., 98 (2007) 028001.

[10] E. Azéma, F. Radjai, R. Peyroux, G. Saussine, in: Traffic and Granular Flow '07, Appert-Rolland et al (Eds.), Springer Berlin Heidelberg, 2009, pp 497-505.

[11] J.-P Bouchaud, M. Cates, P. Claudin, Stress distribution in granular media and non-linear wave equation. Jl. de Phys. I, 5 (1995) 639-656.

[12] Y.P. Vaid, E.K.F. Chung, R.H. Kuerbis, Stress path and steady state, Can.Geo.Jl., 27 (1990) 1–7.

[13] M. Satake, A discrete-mechanical approach to granular materials. Int.Jl.Eng.Sci., 30 (1992) 1525–1533.

[14] Y. Nakata, M. Hyodo, H. Murata, Flow deformation of sands subjected to principal stress rotation, Soil.Found., 38 (1998) 115–128.

[15] M. Yoshimine, K. Ishihara, W. Vargas, Effects of principal stress direction and intermediate principal stress on undrained shear behavior of sand, Soi.Found., 38 (1998) 179–188.

[16] S.J. Antony, B. Stockwell, Influence of particle-scale properties on the charge transfer characteristics in semi-conducting particulate packing: Particle-based Finite Element Analysis, Adv. Powder Tech., 18 (2007) 795-801.

[17] S.J. Antony, Link between single-particle properties and macroscopic properties in particulate assemblies: role of structures within structures, Phil.Trans.Roy.Soc.A, 365 (2007) 2879-2891.

[18] A. Hassanpour, S.J. Antony, M. Ghadiri, Modelling of agglomerate behaviour under shear deformation: Effect of velocity field in high shear mixer granulator on the structure of agglomerates, Adv. Powder Tech., 18 (2007) 803-811.

[19] X. Li, X.S. Li, Micro-macro quantification of the internal structure of granular materials, Jl.Eng.Mech., 135 (2009) 641-656.

[20] J. Duran, Sands, Powders and Grains, Springer-Verlag, New York, 2000.

[21] P.A. Cundall, O.D.L Strack, A discrete numerical model for granular assemblies, Geotech., 29 (1979) 47-65.

[22] S. Lobo-Guerrero, L. Vallejo, Discrete element method evaluation of granular crushing under direct shear test conditions, Journal of Geotechnical and Geoenv.Eng., 131 (2005) 1295-1300.

[23] S.A. Galindo-Torres, D.M. Pedroso, D.J. Williams, L. Li, Breaking processes in three-dimensional bonded granular materials with general shapes. Comput.Phy.Comm., 183 (2012), 266-277.

[24] S.J. Antony, D. Chapman, Probing shear stress distribution within single particle scale inside particulate packing, KONA, 28 (2011)180-188.

[25] A. Munjiza, The combined finite-discrete element methods, Wiley, Chichester, 2004.

[26] M. Pasha, C. Hare, A. Hassanpour and M. Ghadiri, Assessing flowability of small quantities of cohesive powder using distinct element modelling, AIP Conf. Proc. 1542 (2013),959-962.

[27] N. Rahmanian, M. Ghadiri, X. Jia, Seeded granulation, Powder Technology, 206 (2011) 53-62.

[28] N. Rahmanian, M. Ghadiri, X. Jia, F. Stepanek, Characterisation of granule structure and strength made in a high shear granulator, Powd.Tech., 192 (2009), 184-194.

[29] N. Rahmanian, M. Ghadiri, Seeded granulation, KONA, 29 (2011) 3 (also front cover image).

[30] J.W. Dally, W.F. Riley. Experimental Stress Analysis, McGrawHill, Singapore, 1987.

[31] D. Howell, R.P. Behringer, Stress fluctuations in a 2D granular couette experiment: A Continuous Transition. Phy.Rev.Lett., 82(1999) 5241-5244.

[32] D.M. Wood, D. Lesniewska, Stresses in granular materials, Gran.Mat., 13 (2011) 395-415.

[33] N. Rahmanian, Y. Ding, M. Ghadiri, Effect of scale of operation on granule strength in high shear granulators. Chem.Eng.Sci., 63 (2008) 915-923.

[34] C.R. Woodcock, J.S. Mason, Bulk solids handling, Chapman&Hall, Suffolk, 1987.

[35] K. Ramesh, Digital photoelasticity, Springer, New York, 2000.

[36] S.J. Antony, Imaging shear stress distribution and evaluating the stress concentration factor of the human eye, Sci. Rep., Nature Publishing Group, 5 (2015) 8899.

[37] F. Radjai**,** M. Jean, J.J. Moreau, S. Roux, Force distributions in dense two-dimensional granular packing. Phy.Rev.Lett., 77(1997), 274-277.

[38] M.H. Sadd, Elasticity: Theory, Applications and Numerics. Elsevier, Oxford, 2009.

[39] N. Rahmanian, T. El Ganimi, M. Ghadiri, Further investigations on the influence of scale-up of a high shear granulator on the granule properties, Particu., 6 (2013) 627-635.

[40] P. Wang, C. Song, C. Briscoe, K. Wang, H.A. Makse, From force distribution to average coordination number in frictional granular matter, Physi.A, 389 (2010) 3972-3977.

Figure captions

Figure 1: X-ray microtomography images of the central cross section of Durcal granules: (a) seeded granule (b) unseeded granule [27] (c) SEM image of internal structure of about 100 seeded granules of $CaCO_3$ [29].

Figure 2: SEM image of Durcal 65 powder.

Figure 3: The configuration of a circular polariscope [1, 30].

Figure 4: Illustration of particulate samples: (a) granular assemblies and (b) samples of inclusions surrounded by $CaCO_3$ granules and $CaCO_3$ powder.

Figure 5: A schematic diagram of the experimental loading rig.

Figure 6: A schematic diagram of the scanning direction to obtain the data necessary for the evaluation of the shear stress concentration factor.

Figure 7: The maximum shear stress distribution in the FC, SC and random (poly-dispersed) systems under different loading conditions.

Figure 8: The maximum shear stress distribution within inclusions embedded inside different $CaCO_3$ surroundings under different loading conditions.

Figure 9: Maximum shear stress distribution: (a) inclusion alone under axial compression (P=5.9N) (b) Inclusion inside cohesive powder packing under external axial compression (P=41.9N). The scale is the same as that provided in Fig.8.

Figure 10: The major principal stress direction in the FC, SC and random (poly-dispersed) systems under different loading conditions.

Figure 11: The major principal stress direction within inclusions immersed in different $CaCO_3$ particulate media under different loading conditions.

Figure 12: Direction of the major principal stress shown in dotted lines: (a) inclusion disk alone under axial compression (P=5.9N) (b) Inclusion inside cohesive powder packing under external axial compresion (P=41.9N). The scale is the same as that of in Fig.11.

Figure 13: The average value of shear stress concentration factor for the FC, SC and random (poly-dispersed) systems under different load levels.

Figure 14: The shear stress concentration factor for inclusions surrounded by different particulate packing under loading.

Figure 15: Variation of coefficient of variation of k in the particulate beds.

Figure 16: Differential shear stress concentration factor (Δk); (a) Δk at the reference load (5.9 N) and (b) variation of absolute value of Δk with the angle of repose.

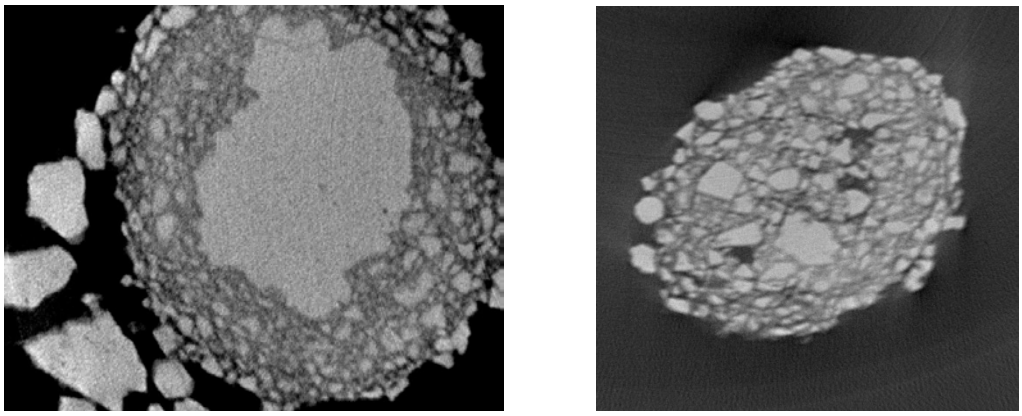

(a) (b)

(c)

Figure 2: X-ray microtomography images of the central cross section of Durcal granules: (a) seeded granule (b) unseeded granule [27] (c) SEM image of internal structure of about 100 seeded granules of $CaCO_3$ [29].

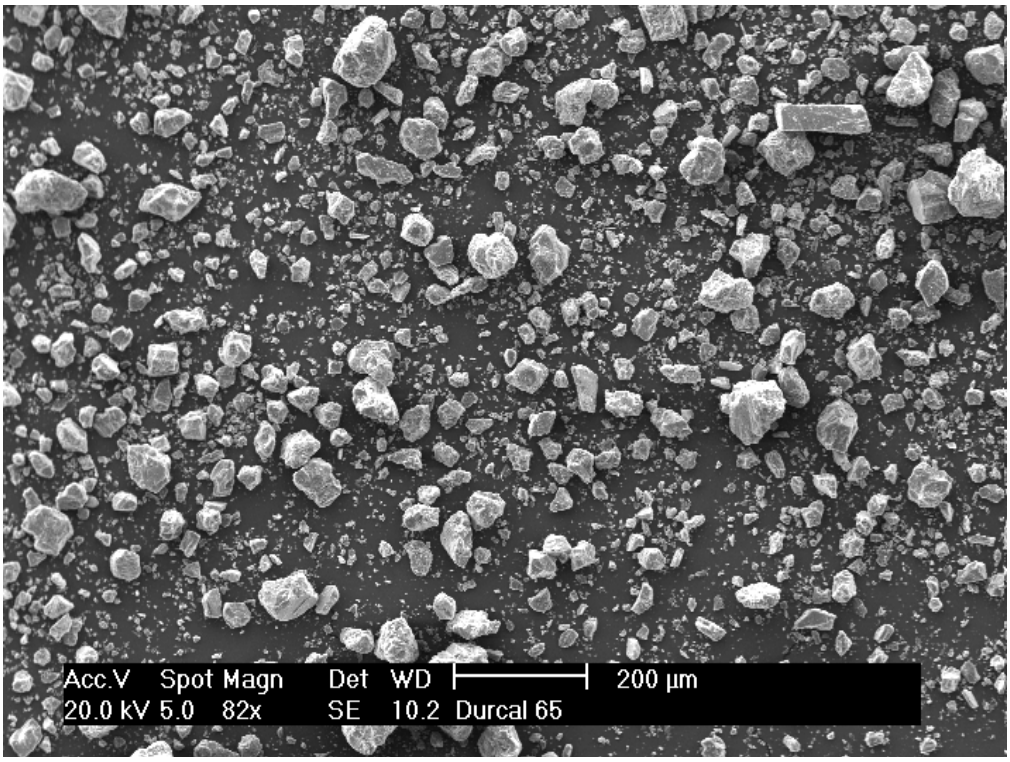

Figure 2: SEM image of Durcal 65 powder.

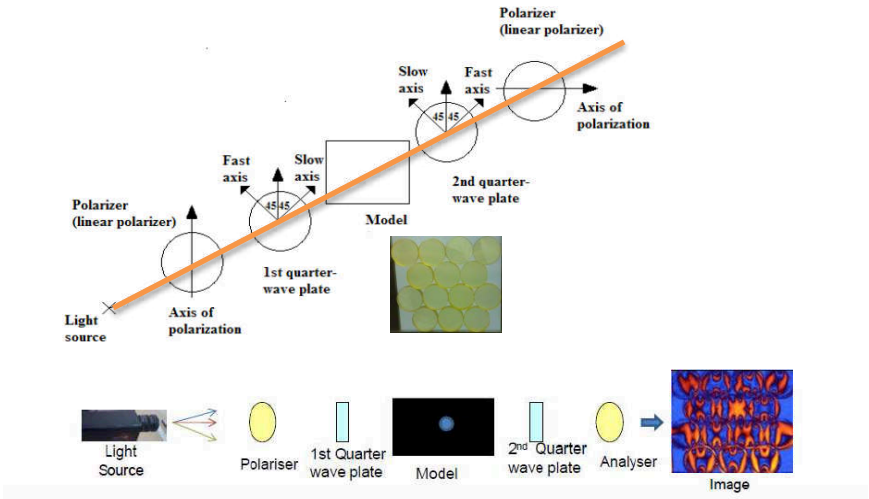

Figure 3: The configuration of a circular polariscope [1, 30].

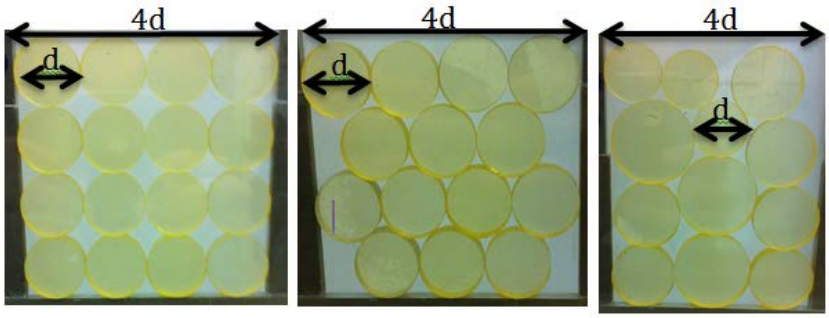

(i) Simple cubic (SC) (ii) Face centred (FC) (iii) Random

(a) Granular packing placed within the compression rig

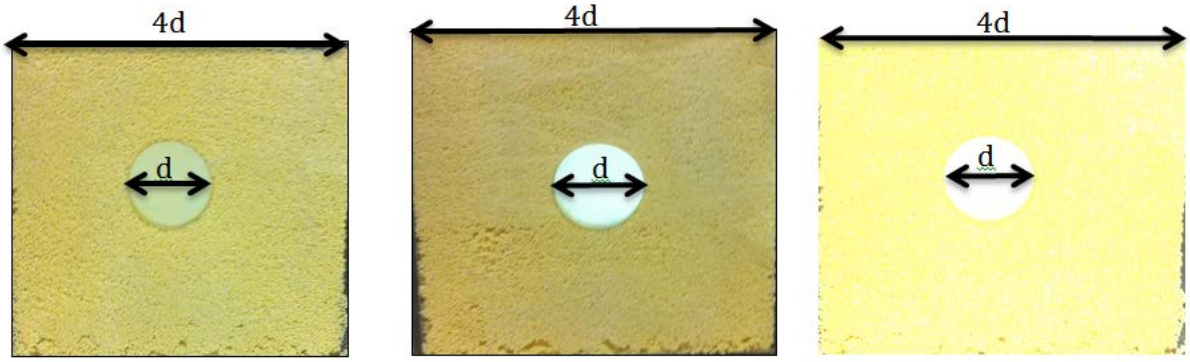

(i) Seeded granules (ii) Unseeded granules (iii) $CaCO_3$ powder

(b) Powder packing with an inclusion inside the compression rig (sample dimension 4dx4d)

Figure 4: Illustration of particulate samples: (a) granular assemblies and (b) samples of inclusions surrounded by $CaCO_3$ granules and $CaCO_3$ powder.

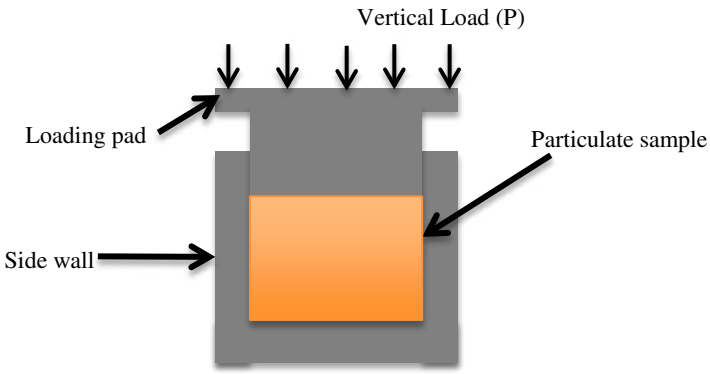

Figure 5: A schematic diagram of the experimental loading rig.

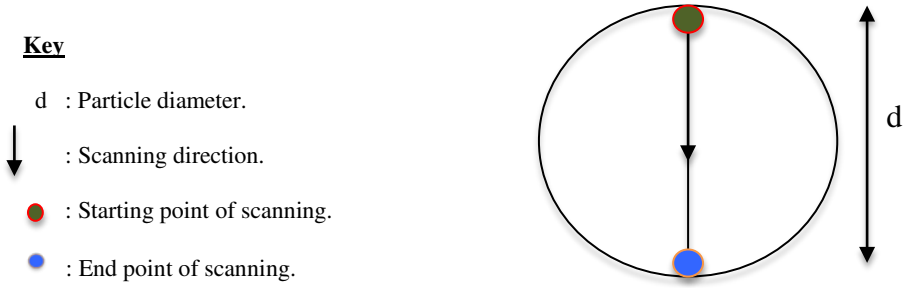

Figure 6: A schematic diagram of the scanning direction to obtain the data necessary for the evaluation of the shear stress concentration factor.

Load (N)	FC	SC	Random	Scale
5.9	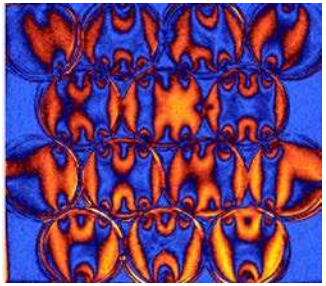	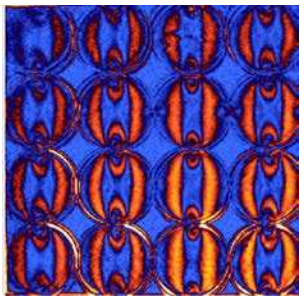	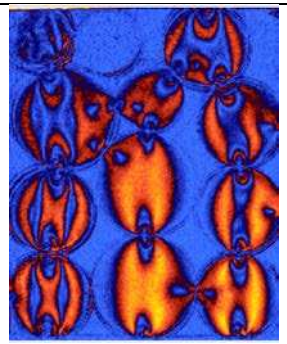	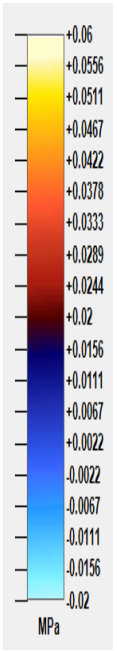
15.7	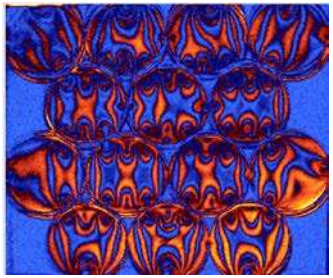	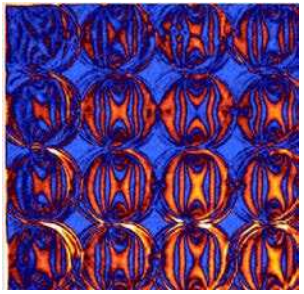	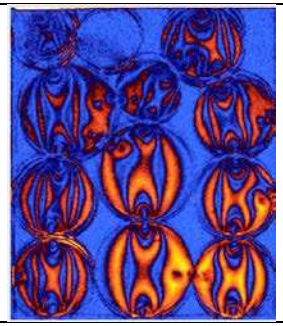	

20.6	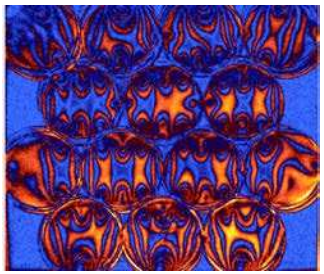	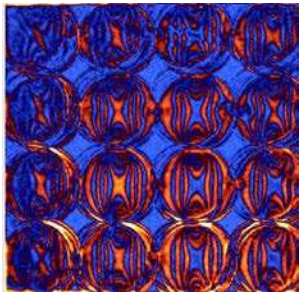	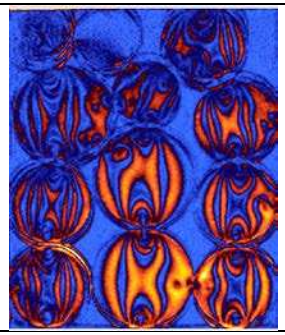	

Figure 7: The maximum shear stress distribution in the FC, SC and random (poly-dispersed) systems under different loading conditions.

Load (N)	unseeded $CaCO_3$	Seeded $CaCO_3$	Cohesive $CaCO_3$	Scale
5.9	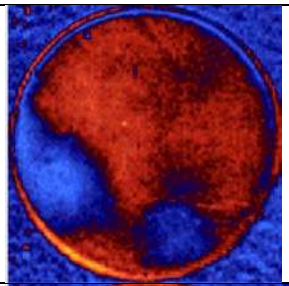	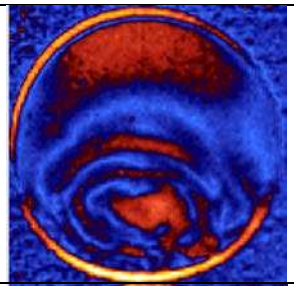	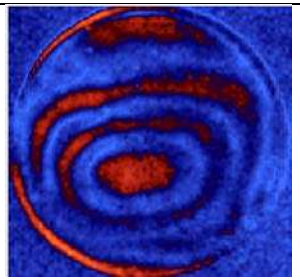	
41.9	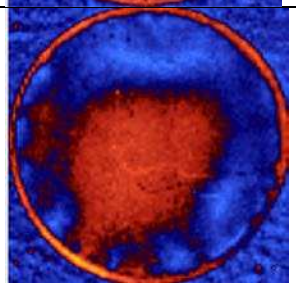	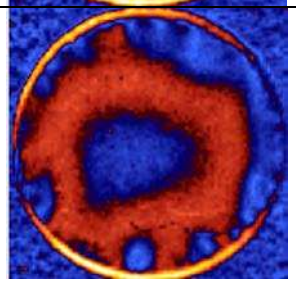	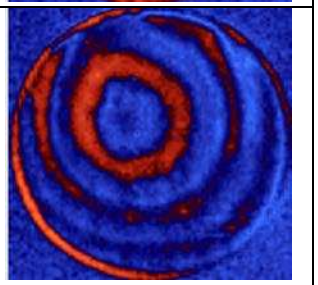	
54.6	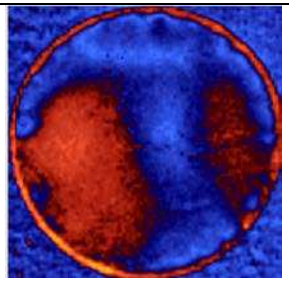	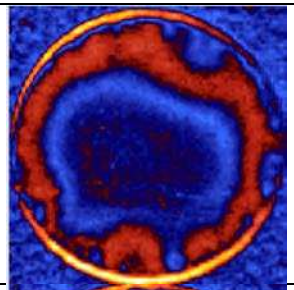	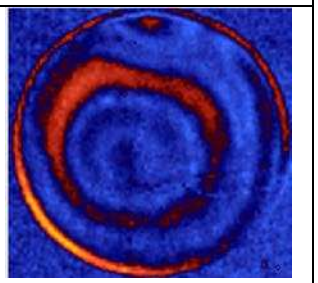	
82.1	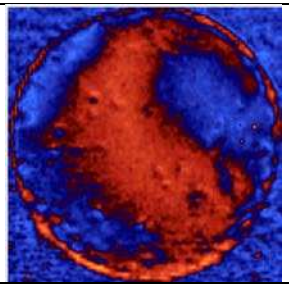	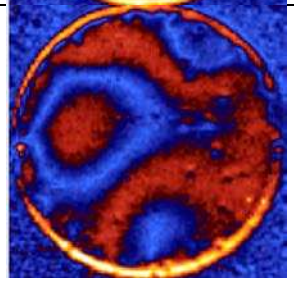	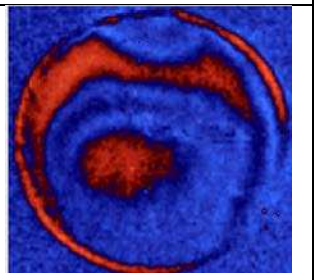	

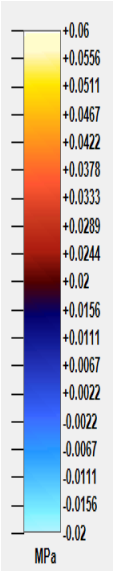

Unloaded at 5.9	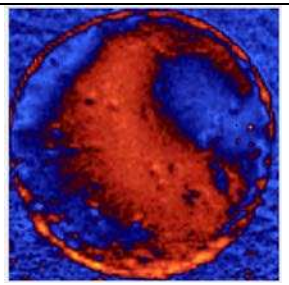	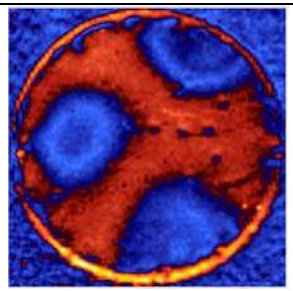	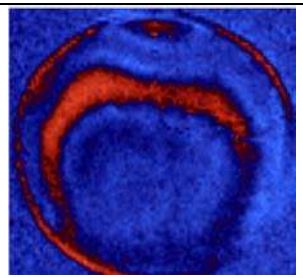	

Figure 8: The maximum shear stress distribution within inclusions embedded inside different $CaCO_3$ surroundings under different loading conditions.

Inclusion without surrounding powder	Inclusion inside cohesive powder bed
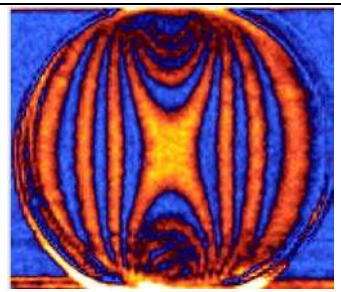	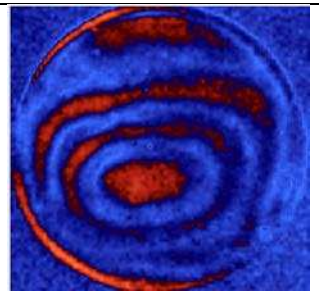

Figure 9: Maximum shear stress distribution: (a) inclusion alone under axial compression (P=5.9N) (b) Inclusion inside cohesive powder packing under external axial compression (P=41.9N). The scale is the same as that provided in Fig.8.

Load (N)	FC	SC	Random	Scale
5.9	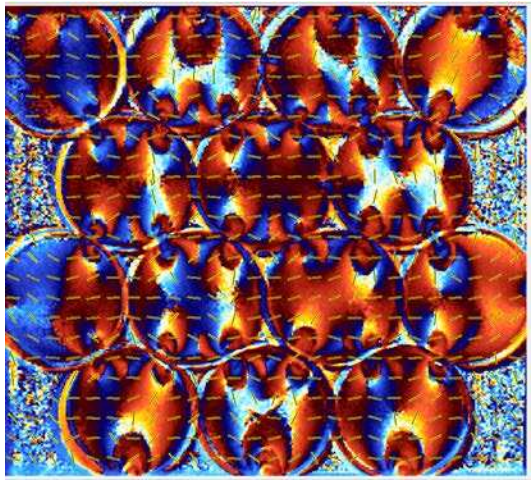	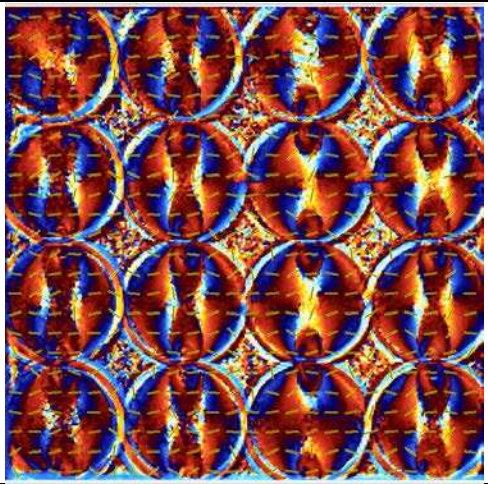	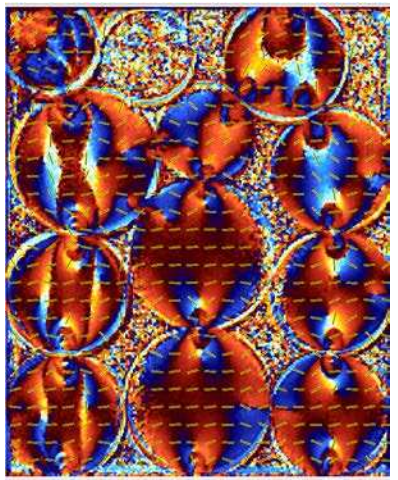	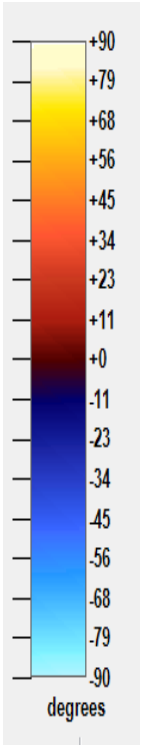
10.8	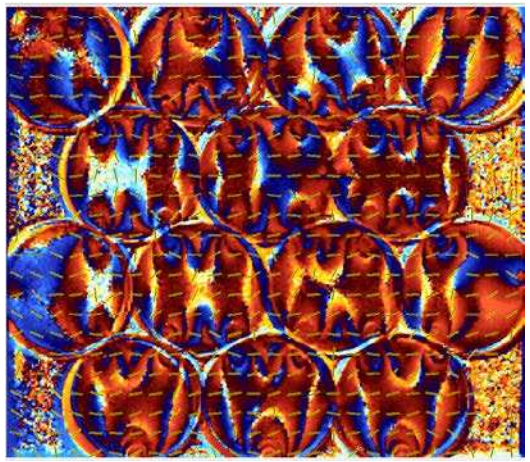	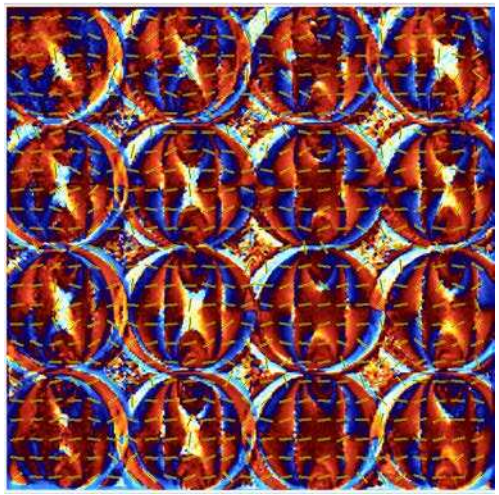	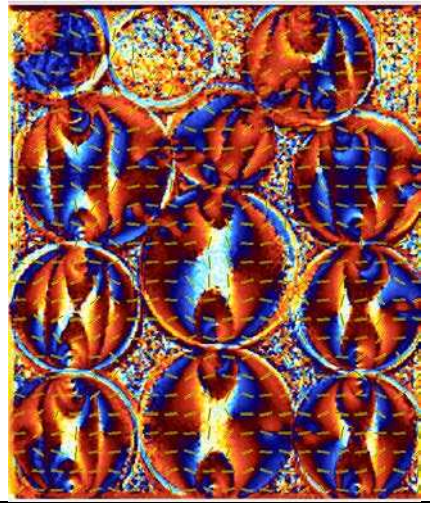	

Figure 10: The major principal stress direction in the FC, SC and random (poly-dispersed) systems under different loading conditions.

Load (N)	Unseeded $CaCO_3$	Seeded $CaCO_3$	Cohesive $CaCO_3$	Scale
5.9	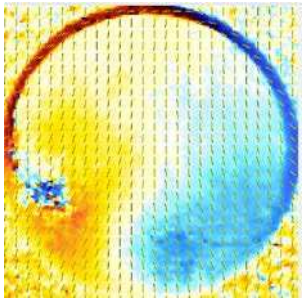	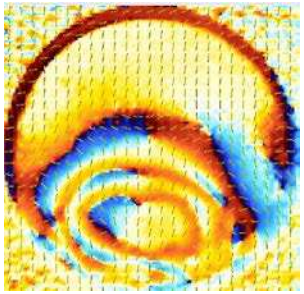	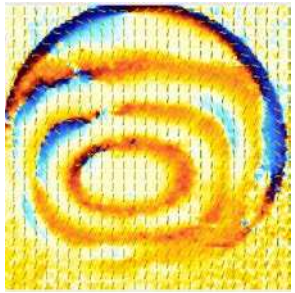	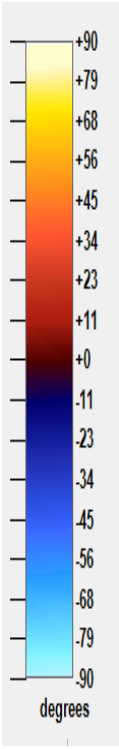
41.9	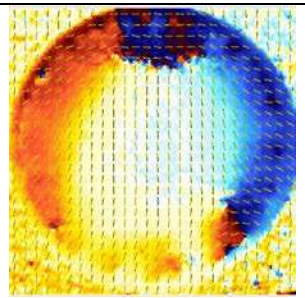	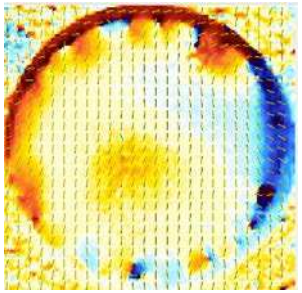	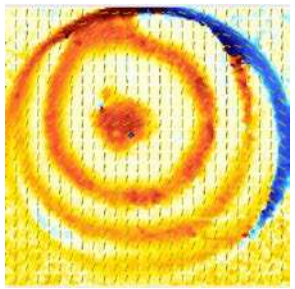	
54.6	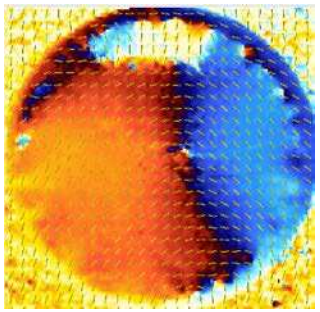	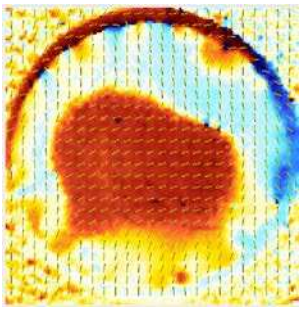	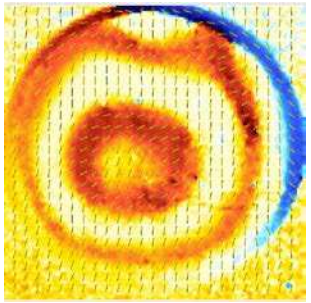	

82.1	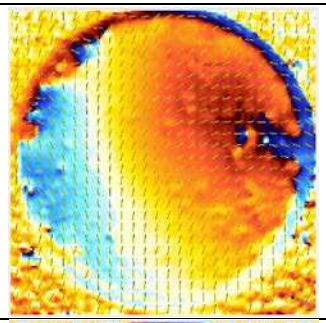	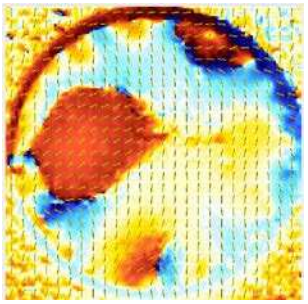	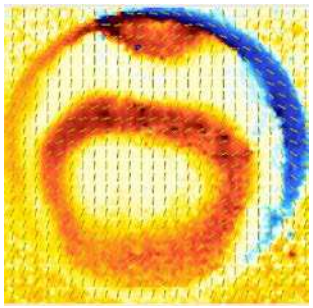	
Unloaded at 5.9	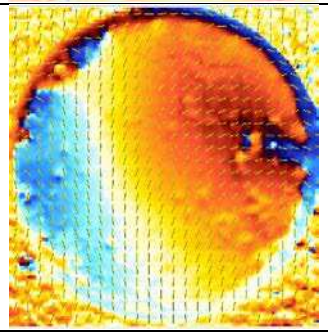	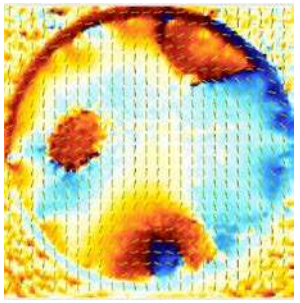	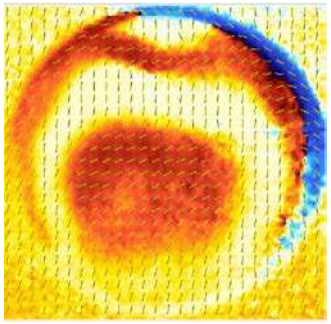	

Figure 11: The major principal stress direction within inclusions immersed in different $CaCO_3$ particulate media under different loading conditions.

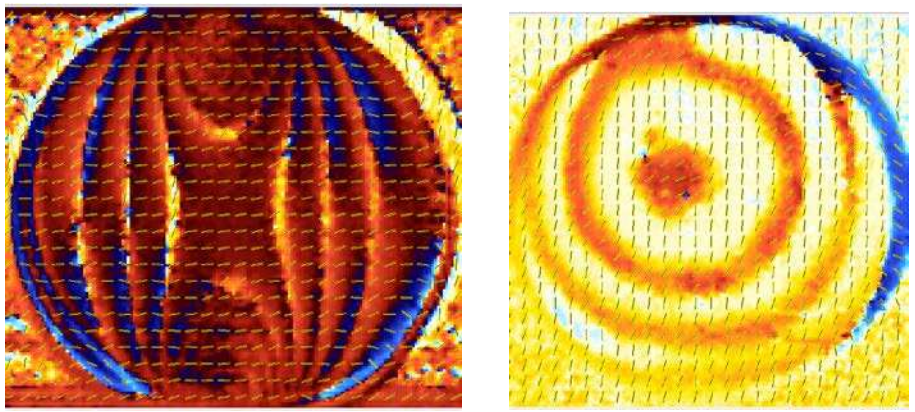

(a) (b)

Figure 12: Direction of the major principal stress shown in dotted lines: (a) inclusion disk alone under axial compression (P=5.9N) (b) Inclusion inside cohesive powder packing under external axial compresion (P=41.9N). The scale is the same as that of in Fig.11.

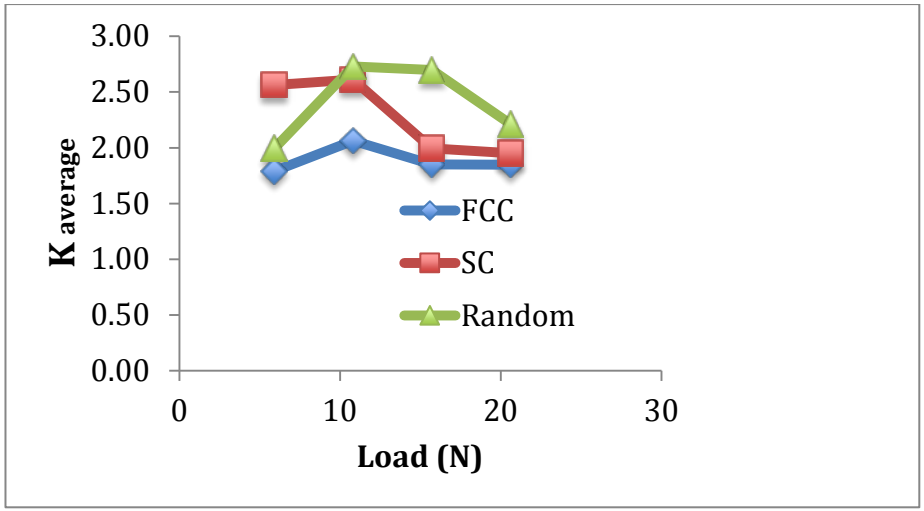

Figure 13: The average value of shear stress concentration factor for the FC, SC and random (poly-dispersed) systems under different load levels.

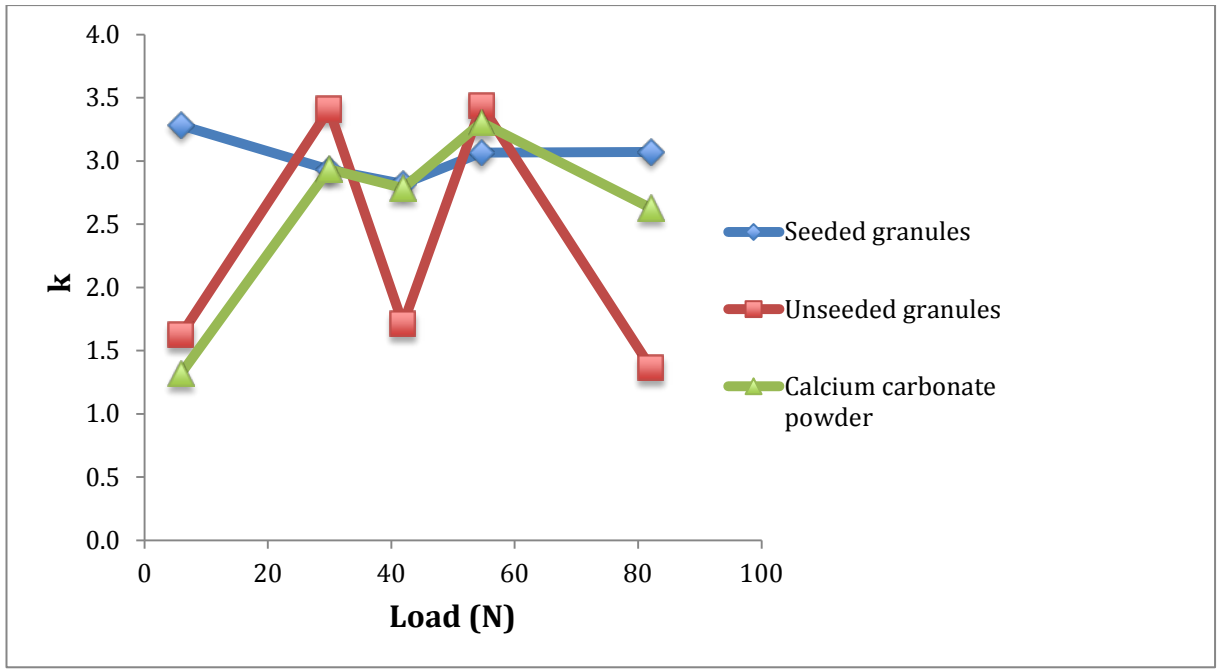

Figure 14: The shear stress concentration factor for inclusions surrounded by different particulate packing under loading.

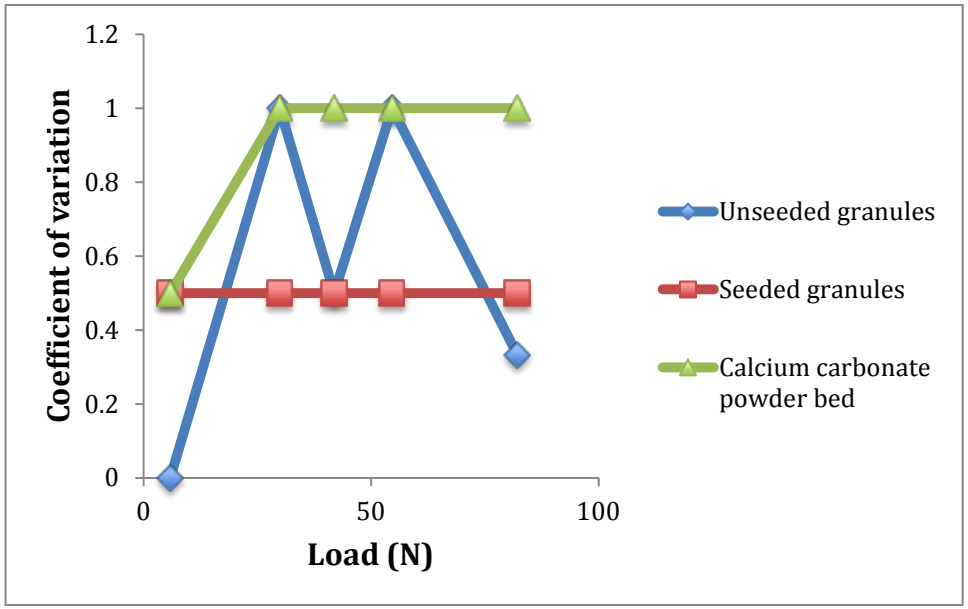

Figure 15: Variation of coefficient of variation of k in the particulate beds.

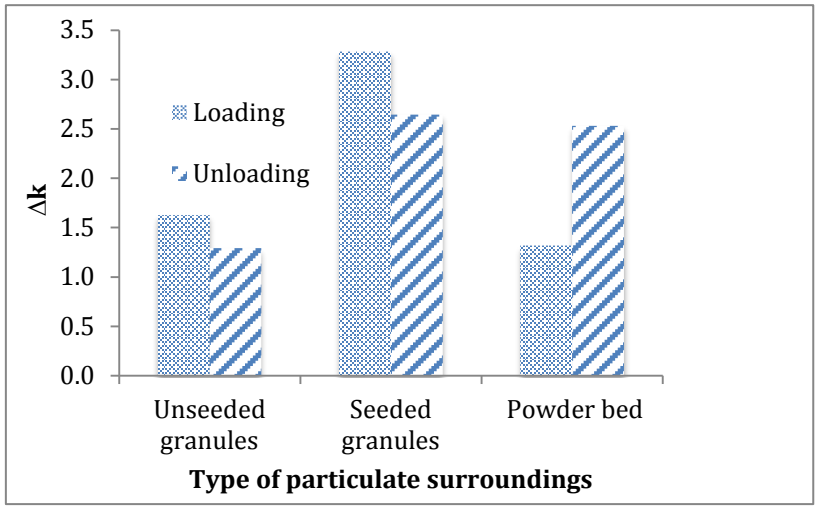

(a)

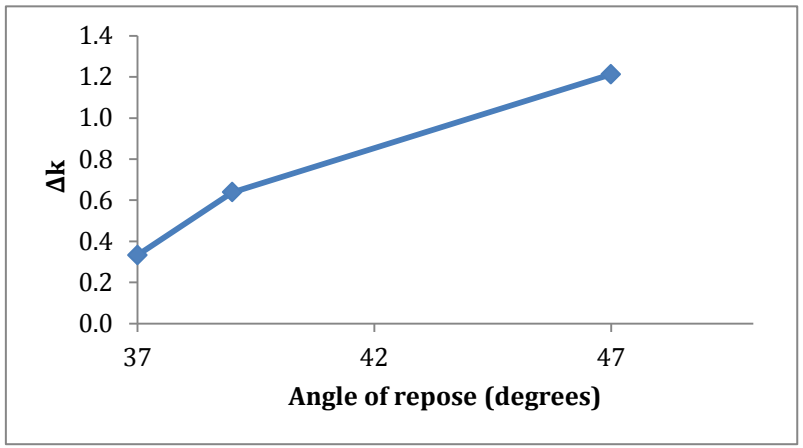

(b)

Figure 16: Differential shear stress concentration factor (Δk); (a) Δk at the reference load (5.9 N) and (b) variation of absolute value of Δk with the angle of repose.